

Spin polarized photocurrent from quantum dots

J. M. Villas-Bôas, Sergio E. Ulloa, and A. O. Govorov
Department of Physics and Astronomy, and Nanoscale and Quantum Phenomena Institute, Ohio University, Athens, Ohio 45701-2979

(Dated: November 8, 2018)

In this paper we show that it is possible to switch the spin polarization of the photocurrent signal obtained from a single self-assembled quantum dot photodiode under the effect of elliptically polarized light by just increasing the light intensity. In the nonlinear mechanism treated here, intense elliptically polarized light creates an effective exchange interaction between the exciton spin states through the biexciton state. This effect can be used as a dynamical switch to invert the spin-polarization of the extracted photocurrent. We further show that the effect persists in realistic ensembles of dots, making this a powerful technique to dynamically generate spin-polarized electrons.

PACS numbers: 72.25.Fe, 78.67.Hc, 42.50.Hz, 03.67.Lx

Classical information processing has been based on charge currents in electronic devices. In the search for quantum alternatives, *spin currents* appear very promising, as typical decoherence times for the spin are much longer than for electron charge. Spin currents are the foundation for “spintronics,” a concept that researchers hope will give additional functionalities and result in improved electronic devices. The spin degree of freedom also constitutes natural qubits, the basic unit in quantum computation and processing, which has been the subject of intense research.^{1,2}

At the same time, recent advances in fabrication, manipulation and probing techniques of semiconductor quantum dots (QDs) have allowed several groups to successfully manipulate coherently the exciton population of a single QD^{3,4,5,6,7,8} using strong resonant laser pulses and different probing techniques. In particular, Zrenner *et al.* have developed a single self-assembled QD photodiode⁶ in which *coherent* population inversion is induced by a strong and carefully tuned optical pulse and probed by the photocurrent signal. In their device the resonant pulse generates an electron-hole pair in the QD, and with the help of an external gate voltage, the carriers can tunnel into nearby contacts. This process generates the photocurrent signal used to monitor the coherent state of the system.

In this paper we model the dynamics of a self-assembled QD photodiode in the presence of *elliptically polarized* laser pulses. We use a density matrix approach that incorporates dipole coupling, multi-exciton states, and dephasing mechanisms introduced by parasitic levels in the structure (associated with the wetting layer). The electron and hole tunneling processes are introduced via rates from a microscopic model of the structure, which includes the electron-hole interaction.⁹ We show that for given elliptical polarization of light we can produce a *spin-polarization reversal* in the photocurrent signal as we increase the pulse area – an effect that can be used as a dynamical spin switch of the generated photocurrent. Moreover, we show that varying intensity of even *circularly* polarized light can control the spin polarization of the photocurrent for large anisotropic exchange;

the effect persists in realistic QD ensembles, allowing the generation of intense spin-polarized current.

An example of those effects can be seen in Fig. 1, showing a contour plot of the degree of spin polarization of the photocurrent signal in a single QD as function of the pulse area and polarization angle ϕ of the laser pulse. The upper panel shows the result for $\phi = \pi/8 \simeq 23^\circ$, where we have high contrast in the spin-polarization reversal. We emphasize that this spin modulation of the photocurrent is achieved for *constant* elliptical polarization, i.e., constant ratio E_-/E_+ , as defined by the angle ϕ , while changing only pulse area (intensity).

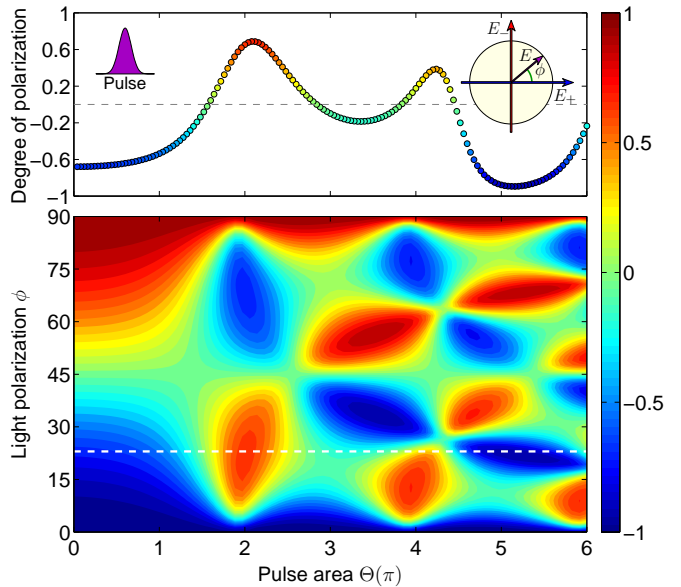


FIG. 1: (Color online) Bottom panel: degree of spin polarization of the photocurrent signal as function of pulse area Θ and polarization angle of the incoming light. Upper panel: results for $\phi = \pi/8 \simeq 23^\circ$ (dashed white line on the contour plot) where local maximum contrast is evident. Notice spin reversal of the photocurrent signal for $\Theta \simeq 2\pi$. Right and left insets show light polarization angle and the 0.5 ps FWHM Gaussian pulse used in the simulation, respectively.

To predict this novel behavior, we have used a realistic

model of the system based on the excitonic levels of a single quantum dot, as summarized in Fig. 2. Using a unitary transformation¹⁰ to remove the fast time-dependent part, one can write

$$H = \delta_{\pm}^X |X_{\pm}\rangle\langle X_{\pm}| + \delta_B^B |B\rangle\langle B| - \frac{1}{2} \left[\Omega_{\pm}^X(t) |0\rangle\langle X_{\pm}| + \Omega_{\pm}^B(t) |X_{\mp}\rangle\langle B| - 2V |X_{-}\rangle\langle X_{+}| + h.c. \right]. \quad (1)$$

Here, X_{\pm} are the excitons with total spins $\pm 1/2$, $\delta_{\pm}^X = \varepsilon_{X_{\pm}} - \hbar\omega$ accounts for the detuning of the exciton from the laser energy $\hbar\omega$, $\delta_B = \varepsilon_B - 2\hbar\omega$ is the two photon biexciton detuning, and $\Omega_{\pm}^X(t) = \langle 0 | \vec{\mu} \cdot \vec{E}_{\pm}(t) | X_{\pm} \rangle / \hbar$, $\Omega_{\pm}^B(t) = \langle X_{\mp} | \vec{\mu} \cdot \vec{E}_{\pm}(t) | B \rangle / \hbar$, are the optical matrix elements, where $\vec{\mu}$ is the electric dipole moment which couples the excitonic transition to the polarization component $\vec{E}_{\pm}(t)$ of the radiation field. The quantity V denotes the anisotropic electron-hole (e - h) exchange interaction which originates either from shape (in III-V materials) or crystal (in II-VI materials) anisotropies of the QD. V provides mixing between spin-defined excitons X_{\pm} , which are directly produced by σ_{\pm} polarized light.^{11,12,13}

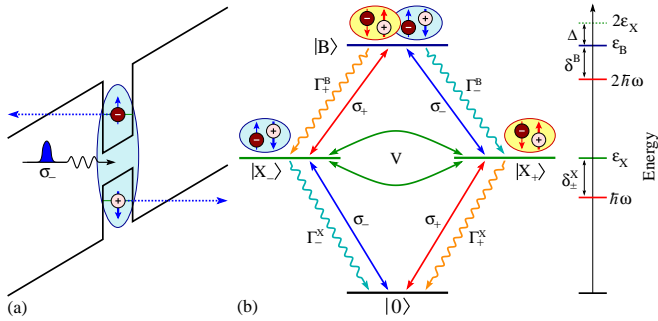


FIG. 2: (Color online) Schematic band structure and level configuration of a single QD photodiode in the presence of pulsed polarized light. (a) A polarized laser pulse creates excitations (exciton, biexciton) in the dot, and an applied gate voltage forces the electrons and holes to tunnel out, generating the measured photocurrent signal. (b) Processes and levels involved in this system: $|X_{\pm}\rangle$ and $|B\rangle$ are the different exciton polarizations and biexciton states.

To obtain the dynamics of the full system we use a density matrix formalism of the form

$$\frac{d\rho}{dt} = -\frac{i}{\hbar} [H, \rho] + L(\rho), \quad (2)$$

where the first term on the right yields the unitary evolution of the quantum system and $L(\rho)$ is the dissipative part of the evolution; we assume the Markovian approximation. Our model considers two types of population decay, one due to the spontaneous decay given by the recombination rate $\Gamma_{\pm}^{\{X,B\}_{\text{rec}}}$, and another due to electron or hole tunneling into the contacts, with rates $\Gamma_{\pm}^{\{X,B\}_{\text{tun}}}$. The total population decay rate for each individual channel can then be written as $\Gamma_{\pm}^{X,B} = \Gamma_{\pm}^{\{X,B\}_{\text{tun}}} + \Gamma_{\pm}^{\{X,B\}_{\text{rec}}}$.

Our simulation uses parameters obtained either from experiments or from realistic estimates. We assume exciton resonant excitation, so that $\delta_{\pm}^X = 0$, while $\delta_B^B = \Delta = 3$ meV is the biexciton binding energy.⁶ The tunneling rates $\Gamma_{\pm}^{\{X,B\}_{\text{tun}}}$ are estimated using a microscopic model,⁹ as function of the external gate voltage, and are in agreement with experimental values; for example, the exciton tunneling time is found to be $\Gamma_{\pm}^X \simeq 12$ ps.⁶

For InGaAs self-assembled QD samples, the e - h exchange interaction is typically a few tens of μ eV, equivalent to an oscillation time between X_{\pm} states of the order of tens of ps. This time is much shorter than the recombination time ($\simeq 1$ ns) so that the QD “visits” both states many times before the exciton recombines. That is the reason why it is so difficult to see polarization of the photoluminescence coming from neutral excitons without the use of a magnetic field, which restores the spin degree of freedom as a good quantum number.¹⁴ In contrast, a photocurrent measurement depends on the tunneling time, which is controllable by an external gate voltage and can be tuned from a few picoseconds and higher. As such, it should be possible to observe spin polarization in the outgoing photocurrent for short tunneling times. For example, for a purely circularly polarized pulse we should be able to produce almost 100% polarized photocurrent just because the readout and manipulation times in this case would be much faster (few picoseconds) than the time for the system to visit the other polarized state (tens of picoseconds) or any other spin dephasing mechanism (usually in the nanosecond scale). It is important to mention that the polarization of nuclear spins in this kind of QD can be an important source of spin dephasing;^{15,16,17} however, the time scale involved in these processes is also much longer than the photocurrent measurement.

Our model also includes the leakage to wetting layers (WL) states, as described in previous work.⁹ This is an important mechanism for the dephasing of the charge state (exciton), but it does *not* affect directly the ratio between the different polarizations of the photocurrent, since the WL states are not spin dependent; as such, their effect turns out to be not as important in the behavior reported here.

Knowing the tunneling rates, the photocurrent signal can be easily computed by integrating in time over all possible channels/modes of particles that tunnel out. As the system is back in the vacuum state $|0\rangle$ when the next pulse arrives, we can write each individual electron spin-components of the photocurrent as

$$I_{\mp} = fq \int_{-\infty}^{\infty} \left[\Gamma_{\pm}^{B_{\text{tun}}} \rho_{BB}(t) + \Gamma_{\pm}^{X_{\text{tun}}} \rho_{X_{\pm}X_{\pm}}(t) \right] dt, \quad (3)$$

where f is the pulse repetition frequency (we use $f = 82$ MHz as in Zrenner’s experiment⁶) and q is the electronic charge. The occupation of each state can be obtained by numerically solving Eq. (2), and then integrating to give each component of the polarized photocurrent (3). The resulting spin-polarized photocurrent signal can then be computed by $P = (I_{+} - I_{-}) / (I_{+} + I_{-})$. Notice that the

spin polarization of the current is associated with the spin of the electron only, as the hole is known to have a rather high spin flip rate due to spin-orbit interaction. As such, the hole loses its spin memory soon after tunneling and only the electron spin remains.

Figure 1 shows a contour plot of typical results as function of the total pulse area $\Theta = \int_{-\infty}^{\infty} \vec{\mu} \cdot \vec{E}(t) dt / \hbar$. Here, $\vec{E}(t) = \vec{E}_+(t) + \vec{E}_-(t)$ is the total pulse amplitude with polarization components $\vec{E}_{\pm}(t)$ and polarization angle $\phi = \tan^{-1}(E_-/E_+)$ of the incoming pulse of Gaussian shape and 0.5 ps FWHM. We can see a rich dependence with polarization angle ϕ , where 0 corresponds to a σ_+ , and 90° to a σ_- pulse as can be seen in the top right inset of Fig. 1. In detail, the upper panel shows results for $\phi = \pi/8 \simeq 23^\circ$, where we can see a maximum contrast in the spin-polarization reversal, going from $\simeq 65\%$ spin down for low laser intensity to $\simeq 65\%$ spin up for pulse area $\Theta \simeq 2\pi$. Notice this large change in photocurrent polarization arises due to the differences in state populations, as controlled by the laser intensity (pulse area), despite the fact that the system is pumped with a *constant* ratio E_-/E_+ , as defined by the angle ϕ .

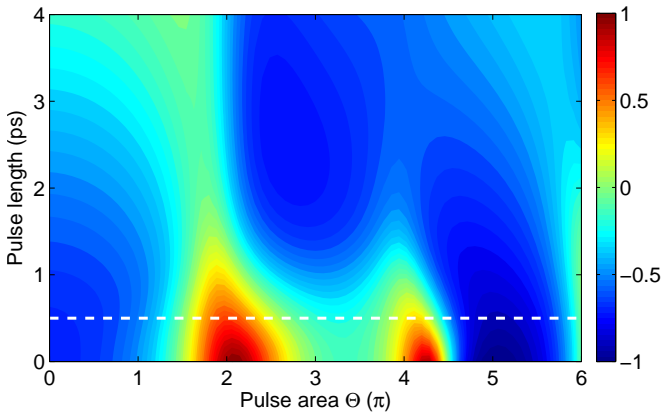


FIG. 3: (Color online) Photocurrent polarization map as function of pulse area Θ and pulse length for elliptically polarized incoming light with phase $\phi = \pi/8 \simeq 23^\circ$, corresponding to the dashed line in Fig. 1. Dashed line here shows pulse length used in Fig. 1. The strong inversion of the signal is suppressed for longer pulses, and the remaining features are due to the small anisotropic e - h exchange interaction ($V = 70 \mu\text{eV}$).

To obtain a more complete picture of this behavior, Fig. 3 shows a contour plot of the polarization signal for the optimal angle $\phi \simeq 23^\circ$ as function of the pulse duration and pulse area. Notice that the spin reversal with Θ occurs only for short pulses. We know from our previous studies that longer pulses reduce the occupation probability of the biexciton state,⁹ which in turn reflected in the photocurrent polarization signal exhibiting smaller or no switching with larger pulse area. For pulses longer than 2 ps the biexciton occupation is negligible, and the features seen in Fig. 3 are caused only by the anisotropic e - h exchange interaction which we assume to be $70 \mu\text{eV}$, as in the experiment by Muller *et*

*al.*¹⁸ For longer pulses, the time to visit the other spin state starts to become important; without the anisotropic e - h exchange interaction no polarization change is seen in Fig. 3 for pulse widths longer than 2 ps (data not shown). This demonstrates that the biexciton plays an essential role in this spin switch device. The biexciton works as an effective exchange channel between the two polarizations due to nonlinear optical interference. In fact, neglecting the biexciton state in the simulation, Fig. 1 changes its color uniformly from bottom to top (increasing angle ϕ) and is basically constant from left to right (increasing laser intensity; data not shown). In that case, the degree of polarization would naturally be proportional to the ratio E_-/E_+ .¹⁹ In the same way, the analogue of Fig. 3 would be of a single color, with the tone being set by the ratio E_-/E_+ .

It is interesting to note that a stronger anisotropic e - h exchange interaction can also result in strong spin switching, even with no elliptical polarization of light. The possibility for such behavior resides in group II-VI materials with strong crystal anisotropy or in large shape anisotropies in typical QDs (such as elongated dots in one direction, even in III-V materials). In that case, a spin switch device develops as well, as one can see in Fig. 4. There we show the degree of photocurrent polarization in a QD as function of exchange interaction V and pulse area Θ achieved by applying a *circularly polarized* σ_+ pulse with FWHM of 1 ps. We notice, for example, that for a QD with $V = 1 \text{ meV}$, as those in Ref. [20], one can achieve the same type of oscillation in the polarization signal of the photocurrent as in the case of the shorter elliptically polarized pulse in a typical (small V) QD.

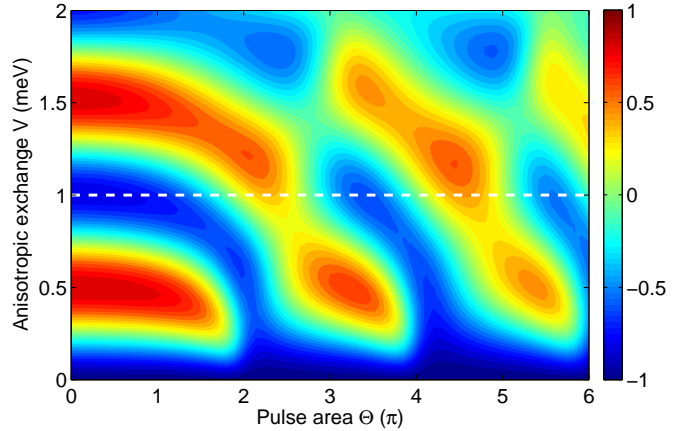


FIG. 4: (Color online) Photocurrent polarization map vs. pulse area and anisotropic e - h exchange interaction V for 1 ps *circularly polarized* pulse σ_+ ($\phi = 0$). For strong exchange interaction $V = 1 \text{ meV}$, dashed line, one can see strong oscillations of the polarization as the pulse area Θ increases.

Most interestingly, it is also possible to observe the predicted effect in QD *ensembles*. The spin-polarized photocurrent response in ensembles would not only make its experimental realization much easier, but it will also open

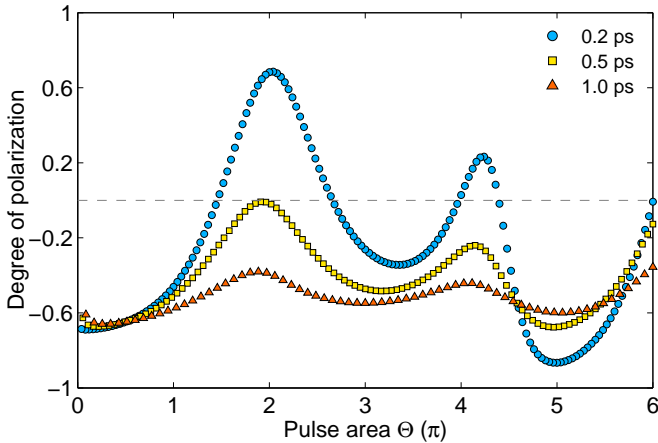


FIG. 5: (Color online) Polarization of the photocurrent signal as function of the pulse area for an ensemble of QDs for three different pulse widths and polarization angle $\phi \simeq 23^\circ$. The Gaussian size distribution has 20% FWHM.

the door for innumerable applications. In an ensemble of QDs we have to address the consequences of their size distribution: QDs with different sizes have different energy levels, so that a laser pulse in resonance with the exciton energy in one dot is detuned with respect to the neighbors. Different sizes also result in different dipole moments, so that the neighbor dots will also oscillate with slightly different Rabi frequency. Another important issue is the shape anisotropy, which would result in different anisotropic e - h exchange interaction. It is known that V can change dramatically (even by 100%) over the dot population, possibly the result of different dot environments, as well as shapes and sizes.

To model the ensemble we then assume a Gaussian distribution of QD sizes such that the photoluminescence of the exciton state would have a broadening of 20 meV, which indeed is a highly homogeneous ensemble, but still feasible in experiments.^{21,22} Directly dependent on that we also assume that the dots have a 20% change in their dipole moment, like in the model used by Borri *et al.*²³ to describe the Rabi oscillations in an ensemble of dots.

The degree of polarization for the ensemble can then be obtained by integrating the contribution of individual dots as $P_{\text{ens}} = \int_0^\infty \int_0^\infty P(\delta(R), \Omega(R), V) f(R) g(V) dR dV$, where f and g describe the corresponding size and V distribution functions. We assume that the detuning and the difference in dipole moments are correlated (as per dot size), while they are uncorrelated with respect to the anisotropic e - h exchange interaction (for which we also assume a Gaussian distribution $g(V)$ with FWHM of $70\mu\text{eV}$ around the typical value $V = 70\mu\text{eV}$).

In Fig. 5 we show the results for three different pulse widths. We can see that the size distribution tends to suppress the effect, as one would expect, but there is a non-zero polarization even for small pulse area. In particular, compare the middle trace here (squares) for 0.5 ps pulse, with the upper panel in Fig. 1. Notice that longer pulses (triangles) exhibit an oscillatory polarization with pulse area, but no signal inversion. However, shorter pulses (circles) restore a great deal of modulation and polarization reversal with Θ , *despite QD ensemble inhomogeneities*. The polarized signal has a strong dependence on the pulse area (for fixed pulse duration), and at around 2π there is a *reversal* in the signal polarization. This is an important and exciting result which reflects nonlinear effects clearly involving the biexciton state. Being able to dynamically invert the spin photocurrent with pumping intensity can prove very useful in controlling the polarization in QDs and associated devices.

We have presented a model to describe non-linear spin-dependent effects in self-assembled QD photodiodes. Our model includes excitons with different polarization and biexciton states, and is based on the density matrix formalism. We show that for an elliptically polarized pulse the photocurrent signal presents a clear inversion of its electron spin component as function of the pulse area for a single QD. We also show that such effect can still be observed in an typical ensemble of dots, which makes it more attractive for device applications.

This work was supported by the Indiana 21st Century Fund, and by the BNNT project at OU.

¹ M. E. Flatté, J. M. Byers, and W. H. Lau, in *Semiconductor Spintronics and Quantum Computation*, edited by D. D. Awschalom, D. Loss, and N. Samarth (Springer, New York, 2002).

² A. Imamoglu, D. D. Awschalom, G. Burkard, D. P. Di Vincenzo, D. Loss, M. Sherwin, and A. Small, Phys. Rev. Lett. **83**, 4204 (1999).

³ T. H. Stievater, Xiaoqin Li, D. G. Steel, D. Gammon, D. S. Katzer, D. Park, C. Piermarocchi, and L. J. Sham, Phys. Rev. Lett. **87**, 133603 (2001).

⁴ H. Kamada, H. Gotoh, J. Temmyo, T. Takagahara, and H. Ando, Phys. Rev. Lett. **87**, 246401 (2001).

⁵ H. Htoon, T. Takagahara, D. Kulik, O. Baklenov, A. L. Holmes, Jr., and C. K. Shih, Phys. Rev. Lett. **88**, 087401

(2002).

⁶ A. Zrenner, E. Beham, S. Stufler, F. Findeis, M. Bichler, and G. Abstreiter, Nature **418**, 612 (2002).

⁷ Q. Q. Wang, A. Muller, P. Bianucci, E. Rossi, Q. K. Xue, T. Takagahara, C. Piermarocchi, A. H. MacDonald, and C. K. Shih, Phys. Rev. B **72**, 035306 (2005).

⁸ S. Stufler, P. Ester, A. Zrenner, and M. Bichler, Phys. Rev. B **72**, 121301(R) (2005).

⁹ J. M. Villas-Boas, S. E. Ulloa, and A. O. Govorov, Phys. Rev. Lett. **94**, 057404 (2005).

¹⁰ J. M. Villas-Boas, A. O. Govorov, and S. E. Ulloa, Phys. Rev. B **69**, 125342 (2004).

¹¹ D. Gammon, E. S. Snow, B. V. Shanabrook, D. S. Katzer, and D. Park, Phys. Rev. Lett. **76**, 3005 (1996).

¹² N. H. Bonadeo, J. Erland, D. Gammon, D. Park, D. S. Katzer, and D. G. Steel, *Science* **282**, 1473 (1998).

¹³ M. Bayer, A. Kuther, A. Forchel, A. Gorbunov, V. B. Timofeev, F. Schafer, J. P. Reithmaier, T. L. Reinecke, and S. N. Walck, *Phys. Rev. Lett.* **82**, 1748 (1999).

¹⁴ M. Kroutvar, Y. Ducommun, D. Heiss, M. Bichler, D. Schuh, G. Abstreiter, and J. J. Finley, *Nature* **432**, 81 (2004).

¹⁵ A. I. Tartakovskii, J. Cahill, M. N. Makhonin, D. M. Whittaker, J-P. R. Wells, A. M. Fox, D. J. Mowbray, M. S. Skolnick, K. M. Groom, M. J. Steer, and M. Hopkinson, *Phys. Rev. Lett.* **93**, 057401 (2004).

¹⁶ P.-F. Braun, X. Marie, L. Lombez, B. Urbaszek, T. Amand, P. Renucci, V. K. Kalevich, K. V. Kavokin, O. Krebs, P. Voisin, and Y. Masumoto, *Phys. Rev. Lett.* **94**, 116601 (2005).

¹⁷ A. S. Bracker, E. A. Stinaff, D. Gammon, M. E. Ware, J. G. Tischler, A. Shabaev, Al. L. Efros, D. Park, D. Gershoni, V. L. Korenev, and I. A. Merkulov, *Phys. Rev. Lett.* **94**, 047402 (2005).

¹⁸ A. Muller, Q. Q. Wang, P. Bianucci, C. K. Shih, and Q. K. Xue, *Appl. Phys. Lett.* **84**, 981 (2004).

¹⁹ F. T. Vasko, *Phys. Rev. B* **70**, 073305 (2004).

²⁰ J. J. Finley, D. J. Mowbray, M. S. Skolnick, A. D. Ashmore, C. Baker, A. F. G. Monte, and M. Hopkinson, *Phys. Rev. B* **66**, 153316 (2002).

²¹ S. Malik, C. Roberts, R. Murray, and M. Pate, *Appl. Phys. Lett.* **71**, 1987 (1997).

²² S. Raymond, S. Studenikin, A. Sachrajda, Z. Wasilewski, S. J. Cheng, W. Sheng, P. Hawrylak, A. Babinski, M. Potemski, G. Ortner, and M. Bayer, *Phys. Rev. Lett.* **92**, 187402 (2004).

²³ P. Borri, W. Langbein, S. Schneider, U. Woggon, R. L. Sellin, D. Ouyang, and D. Bimberg, *Phys. Rev. B* **66**, 081306(R) (2002).